ELSEVIER

International Journal of Mass Spectrometry 207 (2001) 19–29

International Journal of Mass Spectrometry

Determination of analytic potentials from finite element computations

S.E. Barlow*, A.E. Taylor, K. Swanson

W.R. Wiley Environmental Molecular Sciences Lab, Pacific Northwest National Laboratory, P.O. Box 999 (K8-88), Richland, WA 99352, USA

Received 31 August 2000; accepted 6 December 2000

Abstract

We present here a general approach for determining analytic electrical potentials from the results of finite difference calculations. Such an approach allows us to explore effects of realistic electrode structures that are not directly amenable to analytic treatment. We then use this technique to find the effects of various modifications of hyperbolic electrode structures of some practical interest by way of example. (Int J Mass Spectrom 207 (2001) 19–29) © 2001 Elsevier Science B.V.

Keywords: Electrostatics; Ion optics; Ion trap

1. Introduction

The study of motion of charged particles begins with the evaluation of the electric and magnetic fields. Electric fields arise from charge distributions and magnetic fields arise from current distributions. The relationships among the fields, charges, and currents are captured in Maxwell's equations. Once the fields are described properly, dynamical studies using a variety of techniques can be undertaken, see, e.g. Davidson [1]. Any general discussion of particle motion lies beyond the scope of this article. Rather, we focus on the specific problem of evaluating electrostatic fields due to conductors. In many cases of interest, particle dynamics are dominated by these "external" fields. In other cases the electrostatic fields are merely one component of a more complicated problem that may require consideration of magnetic fields, self-fields (e.g. space charge), light fields, etc., in any case, the electrostatic contribution must still be considered. In the compact notation of electricity and magnetism, we are seeking a solution of Laplace's equation:

$$\nabla^2\Phi(\mathbf{r}) = 0 \tag{1}$$

where $\Phi(\mathbf{r})$ is the electrostatic potential at a point $\mathbf{r}$. The force on a charge q at $\mathbf{r}$ is then given by

$$\mathbf{F}(\mathbf{r}) = -q\nabla\Phi(\mathbf{r}) = q\mathbf{E}(\mathbf{r}) \tag{2}$$

where the vector $\mathbf{E}(\mathbf{r})$ is the electric field. One of the properties of the solution of Eq. (1) that we make use of is "uniqueness." This fact is proved in any elementary text on partial differential equations. What it means is that having once found *a* solution for Eq. (1) for a particular set of boundary conditions, it is *the*

* Corresponding author. E-mail: se_barlow@pnl.gov

PII S1387-3806(00)00452-8

solution. In what follows we describe a "recipe" for ensuring that our solutions are correct.

Before proceeding, it is worthwhile to note some important definitions and usages. First, all of the equations here are written in S.I. units unless stated otherwise. Second, the term "potential" is used interchangeably with "electrostatic potential" and "electric potential;" and the term "field" is used interchangeably with "electrostatic field" and "electric field." The potential is a scalar quantity, while the field is a vector one. A third point concerns the use of the term "static." This term implies two things: first we assume that the wavelengths of any electromagnetic field are long compared to the dimensions of the system's size; and second, we assume that any motion is nonrelativistic. For example, a Paul trap with an internal diameter of 2 cm and using a 1 MHz ($\lambda = 300$ M) rf trapping field is essentially an electrostatic problem. By contrast the same electrode structure can be placed in a magnetic field of 1 T and used as a Penning trap for electron storage. In this case the electron cyclotron frequency is $\sim$30 GHz ($\lambda \sim 1$ cm) and therefore electrostatic approximations must be used with great care [2].

The older literature on ion and electron optics is replete with techniques for evaluating the potentials for a variety of electrostatic boundary value problems, see, e.g. Spangenberg [3] or Grivet [4]. Today, the labor required to find the potentials is reduced due to the availability of computing resources. Nonetheless, other aspects of this earlier work can still be usefully employed. For example, a considerable amount of work was done in characterizing electrostatic lenses in analogy to their optical counterparts. The characterization then enabled the application of optical modeling techniques to be taken over almost wholesale. Instrument designers continue to use these techniques to this day [5]. In other applications, the potential may be used directly to find analytic trajectories through the use of Hamiltonian or Lagrangian dynamics [6]. Modern versions of potential solvers [7–10] often also include trajectory calculations as well. (In fact, most currently available codes provide only indirect access to the potentials as we will discuss in the following.) In any case, having an accurate analytic form of the potential is the key to utilizing most of the early work. Finally, as Dahl [10] pointed out in his introduction to the SIMION code, the quality and usefulness of the results of a calculation depend on the insight one brings to the problem. Analytic forms of the potential can be quite useful in this regard.

The increasing availability of computing resources and programs have brought ion trajectory simulations and studies within practical reach of most researchers. Many such studies have been published [6–9] in the rf ion trap literature, for example. Most studies generally fall into one of two categories: either particle motion in an analytic potential is examined or the problem is set up in a finite difference program such as SIMION [10], where the user specifies the boundaries and particles and allows the software to do the work. (Several such programs are compared in a recent review article by Forbes et al. [9]) The articles of Franzen et al. [11], Chu et al. [12], and Razvi et al. [13] provide examples of the analytic potential approach. However, none of these authors give readily implemented procedures for actually finding the potential for real electrodes.

Here we show how data developed by finite difference relaxation calculations, e.g. from the SIMION code, may be employed to find actual and accurate potentials for realistic boundaries. Effects of truncations, gaps, holes, construction errors, etc., are readily included in the analysis. The procedure here is specifically tailored for cylindrical boundary conditions and domains, but can be adapted, in principle, to any orthogonal coordinate system that is convenient. The reader may at first find the mathematical manipulations rather daunting, however, a little study will show that they are readily automated. Much of the tedium associated with actual calculation can be avoided by employing computational aids [14–17]. In Sec. 2, the steps required to find the potential from a finite element calculation are treated in some detail. First, we develop the necessary mathematical machinery, starting with a general solution of Laplace's equation in cylindrical coordinates and proceeding through an expansion in powers of r and z—the multipole expansion. Much of the material of Sec. 2 necessarily revisits discussions found elsewhere, but is included for the sake of completeness. Next we discuss the use

of SIMION [10] for performing the finite element calculations. Once the relaxation calculation is performed, only a limited amount of the data is actually needed, we discuss how one selects an appropriate subset of that data. Finally, we show how the numerical data can be inserted into the analytic forms derived first to find the potential. In the examples of Sec. 3, we examine hyperbolic electrodes and explore the effects of truncation, endcap holes, "trap stretching," ring slits and axial asymmetry on the potential.

2. Solving Laplace's equation in cylindrical coordinates

Advanced texts on electrostatics [18,19] give solutions of Laplace's equation, $\nabla^2\Phi = 0$, in various coordinate systems and these solutions form the starting place for our treatment. However, these solutions require a surface that exactly matches the orthogonal coordinates. For instance, in Cartesian coordinates (x, y, z) planes forming a rectangular prism are required, whereas in cylindrical coordinates (r, θ, z) cylinders or sections of cylinders are used. Similar conditions apply to any other coordinate system one may choose [20]. In these coordinate systems, a solution of Laplace's equation can be effected by the method of "separation of variables" where the partial differential equation separates into two or three ordinary differential equations that can be solved by standard means. The general result is a fearsome looking sum over orthogonal functions (the basis functions). In the familiar Cartesian coordinates, the sum may include sines, cosines, and hyperbolic functions and not coincidently bears a strong similarity to a Fourier series [21]. Moving to cylindrical coordinates, we find Bessel functions appearing; most symbolic manipulation codes include them routinely [14–17].

Although many problems associated with charged particle storage and transport employ cylindrical or approximately cylindrical symmetry, none fully match the rigorous requirements stated previously. In all real systems, various compromises are required: spacing between electrodes, apertures, and construction tolerances all must be considered. Too often, the experimentalist is left to wonder just how large these effects are and

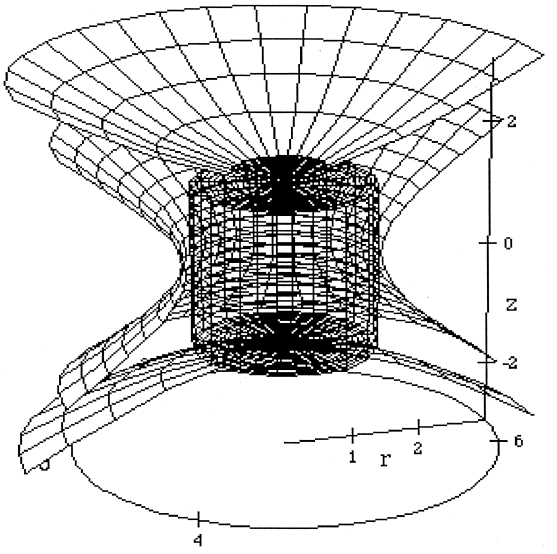

Fig. 1. Wire frame schematic of hyperbolic electrode structure with inscribed cylinder. See the text for discussion.

what are the consequences. A limited amount of work in this direction has been presented by Beatty [22] and Gabrielse et al. [23], but their approaches lie outside the resources of most workers. We have chosen instead to tackle the problem with the widely used SIMION [10] code, but it is only one of several that are available. The numerical methods of codes like SIMION tend to produce less precise results than the techniques of Beatty [22] or Gabrielse et al. [23–24]. For this loss of precision, the user gets a relatively easily used code that has enormous flexibility for defining boundary conditions. Electrodes, gaps, and apertures are all readily described, often through a graphical user interface (GUI) that allows one to visualize the system. Most of the work associated with the calculations, goes into accurately inputting the boundaries. (It does require some practise to use these codes effectively, particularly in learning to scale the input to maximize the effective resolution and at the same time minimizing numerical distortion.)

2.1. Laplace's equation in cylindrical coordinates

As stated previously we are restricting ourselves here to cylindrically symmetric systems. Further, we shall only be concerned with the "interior problem,"

i.e. all solutions of interest will contain the origin. (Neither of these restrictions is essential. The results here can be generalized considerably, but at the cost of additional analysis.) Consider the cylinder illustrated in Fig. 1, the cylinder is centered on the $r = 0$ axis and has a radius c. The bottom and top of the cylinder are located at z_b and z_t, respectively; further, the cylinder contains no conductors, except possibly at the wall. The solution to Laplace's equation in this volume can then be written [18,19] as

$$\Phi(r, \theta, z) = \sum_{s=0}^{\infty} \left\{ \begin{array}{l} \alpha_{1,s} \cos\left[\dfrac{(2s+1)\pi(2z - z_t - z_b)}{2(z_t - z_b)}\right] I_0\left[\dfrac{(2s+1)\pi r}{2(z_t - z_b)}\right] \\ \quad + \alpha_{2,s} \sin\left[\dfrac{2\pi s(2z - z_t - z_b)}{z_t - z_b}\right] I_0\left[\dfrac{4s\pi r}{z_t - z_b}\right] \end{array} \right\} + \sum_{s=1}^{\infty} \left\{ \begin{array}{l} \alpha_{3,s} \sinh\left[\dfrac{(z - z_t)j_s}{c}\right] J_0\left[\dfrac{j_s r}{c}\right] \\ - \alpha_{4,s} \sinh\left[\dfrac{(z - z_b)j_s}{c}\right] J_0\left[\dfrac{j_s r}{c}\right] \end{array} \right\} \tag{3}$$

Here, $J_0(x)$ is the Bessel function of the first kind of order 0; and $I_0(x)$ is the modified Bessel function of order zero. (See, e.g., Olver [26] or Watson [26] for details.) The symbol j_s is the sth zero of $J_0(x)$. If we designate the potential on the top of the cylinder as $V_t(r, z = z_t)$, that on the bottom as $V_b(r, z = z_b)$ and on the side as $V_r(r = c, z)$ we find for the α's:

$$\alpha_{1,s} = \frac{2}{(z_t - z_b) I_0\left[\dfrac{(2s+1)\pi c}{2(z_t - z_b)}\right]} \int_{z_b}^{z_t} V_r(z) \cos\left[\frac{(2s+1)\pi(2z - z_b - z_t)}{2(z_t - z_b)}\right] dz, \tag{4}$$

$$\alpha_{2,s} = \frac{2}{(z_t - z_b) I_0\left[\dfrac{4s\pi c}{z_t - z_b}\right]} \int_{z_b}^{z_t} V_r(z) \sin\left[\frac{2s\pi[2z - z_b - z_t]}{z_t - z_b}\right] dz, \tag{5}$$

$$\alpha_{3,s} = \frac{2}{c^2 \sinh\left(\dfrac{(z_t - z_b)j_s}{c}\right)[J_1(j_s)]^2} \int_0^c V_b(r) J_0\left(\frac{j_s r}{c}\right) r\, dr \tag{6}$$

$$\alpha_{4,s} = \frac{2}{c^2 \sinh\left(\dfrac{(z_t - z_b)j_s}{c}\right)[J_1(j_s)]^2} \int_0^c V_t(r) J_0\left(\frac{j_s r}{c}\right) r\, dr \tag{7}$$

where we use $V(r, z)$ found from the finite difference calculations as described in the following. The α's tend to become rapidly small with s, so we find that only a few of these terms need to be explicitly evaluated unless we are interested in the solution very near a boundary.

2.2. Multipole expansion of Laplace's equation

For the cylindrically symmetric case, Laplace's equation is written as

$$\frac{1}{r}\frac{\partial}{\partial r}\left(r \frac{\partial}{\partial r}\Phi\right) + \frac{\partial^2}{\partial z^2}\Phi = 0 \tag{8}$$

The solution of Eq. (8) can be written in terms of a series expansion using Legendre polynomials, see, e.g. Franzen et al. [11], p. 146. The Legendre polynomials can be in turn be expressed as simple polynomials in r and z. These polynomials have the property that for each term of the nth polynomial, $r^j z^k$; $j + k = n$. This form of the solution to Eq. (8)

Table 1
Solutions of cylindrically symmetric LaPlace's equation through sixth order; see the text for further discussion

Order	Coef.	Form (Φ_n)	Name
0	C_0	1	Monopole
1	C_1/c	z	Dipole
2	C_2/c^2	$-\frac{1}{2}r^2 + z^2$	Quadrupole
3	C_3/c^3	$-\frac{3}{2}r^2z + z^3$	Hexapole
4	C_4/c^4	$\frac{3}{8}r^4 - 3r^2z^2 + z^4$	Octopole
5	C_5/c^5	$\frac{15}{8}r^4z - 5r^2z^3 + z^5$	Decapole
6	C_6/c^6	$-\frac{5}{16}r^6 + \frac{45}{8}r^4z^2 - \frac{15}{2}r^2z^4 + z^6$	Dodecapole

is known as the "multipole expansion." Table 1 lists the multipole expansion solutions of Eq. (8) through the sixth order. Notice that every order of z appears, but owing to cylindrical symmetry, only even powers of r are present. Also notice that we have chosen the coefficients of z^n equal to unity in each case. We did this to simplify our later notation, not because it is otherwise significant. In a similar vein, we choose to normalize the solutions by c, the radius of our cylinder's surface in Fig. 1, this too is a matter of convenience. The total potential can then be written as

$$\Phi = V \sum_{n=0}^{\infty} \frac{C_n}{r_0^n} \Phi_n \tag{9}$$

Here, V is some applied potential and r_0 is a characteristic radius that scales the actual size of the system. The constants, C_n, depend only on the relative shapes and dimensions of our boundary conditions and as such are insensitive to scaling. Finally, we have truncated the expansion at the sixth order, but it can easily be extended to higher orders. Since each of the terms in Table 1 are linearly independent of the others, the coefficients, i.e., the C's, can now be found from Eq. (3). This is done most simply by setting $r = 0$ and expanding the result in a Taylor series about $z = 0$. The resulting equations through the sixth order are

$$C_0 = \left\{ \sum_{s=0}^{\infty} \left(\alpha_{1,s} \cos\left[\frac{\{2s+1\}\pi\{z_t + z_b\}}{z_t - z_b}\right] - \alpha_{2,s} \sin\left[\frac{2s\pi\{z_t + z_b\}}{z_t - z_b}\right]\right) + \sum_{s=1}^{\infty} \left(\alpha_{3,s} \sinh\left[\frac{z_t j_s}{c}\right] - \alpha_{4,s} \sinh\left[\frac{z_b j_s}{c}\right]\right) \right\} \tag{10}$$

$$C_1 = \left\{ \frac{\pi c}{(z_t - z_b)} \sum_{s=0}^{\infty} \left(\alpha_{1,s}[2s+1] \sin\left[\frac{\{2s+1\}\pi\{z_t + z_b\}}{z_t - z_b}\right] + 4\alpha_{2,s} s \cos\left[\frac{2s\pi\{z_t + z_b\}}{z_t - z_b}\right] \right) + \sum_{s=1}^{\infty} \left(-\alpha_{3,s} \cosh\left[\frac{z_t j_s}{c}\right] j_s + \alpha_{4,s} \cosh\left[\frac{z_b j_s}{c}\right] j_s \right) \right\} \tag{11}$$

$$C_2 = \left\{ \frac{\pi^2 c^2}{(z_t - z_b)^2} \sum_{s=0}^{\infty} \left(-\frac{1}{2}\alpha_{1,s}[2s+1]^2 \cos\left[\frac{\{2s+1\}\pi\{z_t + z_b\}}{z_t - z_b}\right] - 8\alpha_{2,s} s^2 \sin\left[\frac{2s\pi\{z_t + z_b\}}{z_t - z_b}\right] \right) - \frac{1}{2} \sum_{s=1}^{\infty} \left(\left\{ \alpha_{3,s} \sinh\left[\frac{z_t j_s}{c}\right] - \alpha_{4,s} \sinh\left[\frac{z_b j_s}{c}\right] \right\} j_s^2 \right) \right\} \tag{12}$$

$$C_3 = \left\{ \frac{\pi^3 c^3}{(z_t - z_b)^3} \sum_{s=0}^{\infty} \left(\frac{1}{6}\alpha_{1,s}[2s+1]^3 \sin\left[\frac{\{2s+1\}\pi\{z_t+z_b\}}{z_t - z_b}\right] + \frac{32}{3}\alpha_{2,s}s^3 \cos\left[\frac{2s\pi\{z_t+z_b\}}{z_t - z_b}\right] \right) + \frac{1}{6}\sum_{s=1}^{\infty}\left(\alpha_{3,s}\cosh\left[\frac{z_t j_s}{c}\right]j_s^3 - \alpha_{4,s}\cosh\left[\frac{z_b j_s}{c}\right]j_s^3\right) \right\} \tag{13}$$

$$C_4 = \left\{ \frac{\pi^4 c^4}{(z_t - z_b)^4} \sum_{s=0}^{\infty} \left(\frac{1}{24}\alpha_{1,s}[2s+1]^4 \cos\left[\frac{\{2s+1\}\pi\{z_t+z_b\}}{z_t - z_b}\right] - \frac{332}{3}\alpha_{2,s}s^4 \sin\left[\frac{2s\pi\{z_t+z_b\}}{z_t - z_b}\right] \right) + \frac{1}{24}\sum_{s=1}^{\infty}\left(\alpha_{3,s}j_s^4\sinh\left[\frac{z_t j_s}{c}\right] - \alpha_{4,s}j_s^4\sinh\left[\frac{z_b j_s}{c}\right]\right) \right\} \tag{14}$$

$$C_5 = \left\{ \frac{\pi^5 c^5}{(z_t - z_b)^5} \sum_{s=0}^{\infty} \left(\frac{1}{120}\alpha_{1,s}[2s+1]^5 \sin\left[\frac{\{2s+1\}\pi\{z_t+z_b\}}{z_t - z_b}\right] - \frac{128}{15}\alpha_{2,s}s^5 \cos\left[\frac{2s\pi\{z_t+z_b\}}{z_t - z_b}\right] \right) - \frac{1}{120}\sum_{s=1}^{\infty}\left(\alpha_{3,s}\cosh\left[\frac{z_t j_s}{c}\right]j_s^5 - \alpha_{4,s}\cosh\left[\frac{z_b j_s}{c}\right]j_s^5\right) \right\} \tag{15}$$

$$C_6 = \left\{ \frac{\pi^6 c^6}{(z_t - z_b)^6} \sum_{s=0}^{\infty} \left(-\frac{1}{720}\alpha_{1,s}[2s+1]^6 \cos\left[\frac{\{2s+1\}\pi\{z_t+z_b\}}{z_t - z_b}\right] - \frac{256}{45}\alpha_{2,s}s^6 \sin\left[\frac{2s\pi\{z_t+z_b\}}{z_t - z_b}\right] \right) - \frac{1}{720}\sum_{s=1}^{\infty}\left(\alpha_{3,s}j_s^6\sinh\left[\frac{z_t j_s}{c}\right] - \alpha_{4,s}j_s^6\sinh\left[\frac{z_b j_s}{c}\right]\right) \right\} \tag{16}$$

Readers who are interested in employing the techniques described here are encouraged to derive this set of equations for themselves. We have found the use of a symbolic manipulation program to be helpful [14–17].

The development to this point is quite general, requiring only cylindrical symmetry and the construction of a cylindrical surface centered on the $r = 0$ axis and interior to the boundaries. For specific applications the choice of the $z = 0$ plane is crucial, because of the Taylor series inherent in the multipole expansion. Once the values of C_i are found for Table 1, they are specific to the particular origin we chose. A coordinate transform to a new origin requires re-evaluation of the C's to ensure that the terms in the expansion remain linearly independent. This point is clear if we substitute $z \rightarrow z' + a$ into the formulae of Table 1. We see that each higher term is "contaminated" with lower order ones and the desirable features of the multipole separation are lost. From a practical standpoint, the choice of origin may be clear from the problem or may require some experimenta-

tion. For instance, in ion trap problems there is generally a plane where the axial electric field is zero or nearly so; this can be chosen as the $z = 0$ plane as ions will oscillate about this plane. Particular questions may well dictate the choice of a different $z = 0$ plane. We note that in the classic texts of Smythe [18] and Jackson [19], both authors choose $z_b = 0$.

Once the cylindrical surface and the origin are defined, Eq. (3) provides a complete solution inside the cylinder. However, unless the cylinder's walls are also electrodes, we may wish to know how the potential behaves outside of our cylinder. This question can not be answered by Eq. (3). On the other hand, the coefficients and formulae of Table 1 are valid in the entire domain of the original relaxation calculation with respect to the origins used in finding the C_i's. The only restrictions are at or inside electrodes themselves. Care must be exercised when attempting to apply the results far from the origin where the higher order terms can utterly dominate the fields.

From the structures of Eqs. (3)–(7) it is apparent that a good deal of simplification will result when a plane of symmetry exists perpendicular to the z axis. If the plane of symmetry exists at $z = 0$, we can replace $z_b = -z_t$; $\alpha_{2,s} = 0$; $\alpha_{4,s} = -\alpha_{3,s}$; and $C_{\text{odd}} = 0$. However, by not enforcing symmetry when it is nominally present, we can identify numerical problems. Ultimately, we find that all finite element calculations are subject to errors of one sort or another. Testing for and finding the error limits provides guidance about the accuracy to which this approach can be applied.

2.3. Setting up the problem in SIMION

By now, SIMION [10] is widely employed in the design of ion optics and for studying ion trajectories in mass spectrometers of various sorts. The discussion here moves in a direction not visualized by the program's designers, but nonetheless is also a capability. (There is nothing particular to SIMION that makes it a requirement for the work described here, but some sort of numerical solution of the actual boundary value problem is needed.)

SIMION works on an evenly spaced Cartesian grid. When cylindrical symmetry is invoked, the Laplace solver is changed to reflect this (see Dahl [10], Appendix E). The user defines electrode structures on this grid using either an input file or through the GUI. The user also specifies the potential of each electrode. Once electrodes and potentials are specified, the program performs iteratively a series of "relaxation" calculations to find the potential at each grid point. When a specific convergence is reached, the program declares the problem "solved," and the calculated potential at each point on the grid is stored in a "potential array" or PA file.

A major challenge in employing finite difference calculations is to find a resolution and scaling factor to adequately capture features one wishes to include in the model. For instance, in modeling hyperbolic electrodes, it may be necessary to rescale the actual structure in order to reflect the symmetries and specific geometric features such as the ratio of the endcap spacing to ring diameter more accurately (see Fig. 2). We have found that rescaling improves accuracy.

Second, a resolution must be chosen to permit computation of particular features. For example, in the trap calculations described in the following, we are concerned with the effects of the holes in the endcaps. For these to be modeled correctly, the hole radius must encompass at least several grid points. After a considerable amount of work we found grid sizes of about 1000×2000 (radial and axial) points gave excellent results. No improvement was found when doubling the array size but the array was adequate to allow us to incorporate the smallest features in which we were interested. (Actually cutting the array size in half produced little change as well.) In particular, our endcap holes spanned about 30 radial grid points. Accuracy was also improved by setting the potential to 1000 V, instead of 1 V, this artifice permitted the program to work with larger numbers thereby reducing the roundoff error. Quality was judged in two ways, first we examined the change in the potentials at selected points as the array size was changed; and second we examined how well the axial symmetry, which we did not enforce, was

reproduced in the cases of the symmetric trap geometries.

2.4. Extracting potentials

In order to apply the developments of Sec. 2.2 to our relaxation calculation, we need to first define an inscribed cylinder, see Fig. 1. We would like this cylinder to be as large as is practical, because maximizing the number of points used in the numerical integrations of Eqs. (4)–(7) improves the accuracy. When employing SIMION [10] we are faced with the additional practical difficulties of actually extracting the potential values from the PA files. These difficulties are twofold: first we must identify the appropriate elements in the array and second we must manipulate large files. For high resolution calculations, the file size may exceed the capacity of standard spreadsheet programs. To deal with these problems we wrote a small program with a graphical interface. This program allows the user to specify which set of points, in the potential file to extract, e.g. $(r = c, z_b) \cdots (r = c, z_t)$; and it also shows a simple graph of the potential. Once the appropriate set of points has been identified, the program writes them in a format that can be read by most spreadsheet programs. This program and some supporting documentation is available from the Environmental Molecular Sciences Laboratory (EMSL) website [30].

After the arrays are extracted to define $V_r(z)$, $V_b(r)$, and $V_t(r)$, they should first be examined carefully to ensure that they do not inadvertently overlap actual electrode structures. The clue is a region of points whose potential value is that of an electrode. With the complex electrode structures for which the techniques here are most useful, this may mean that points of the conductors actually intrude into the cylindrical volume even if this is not apparent from the GUI. Using such surfaces will produce inaccurate results. For purposes of checking the calculations, it is also useful to extract one or more additional potential lines (e.g. the $r = 0$ axis), the value of the potential along these additional lines can then be compared to the results of Eq. (9).

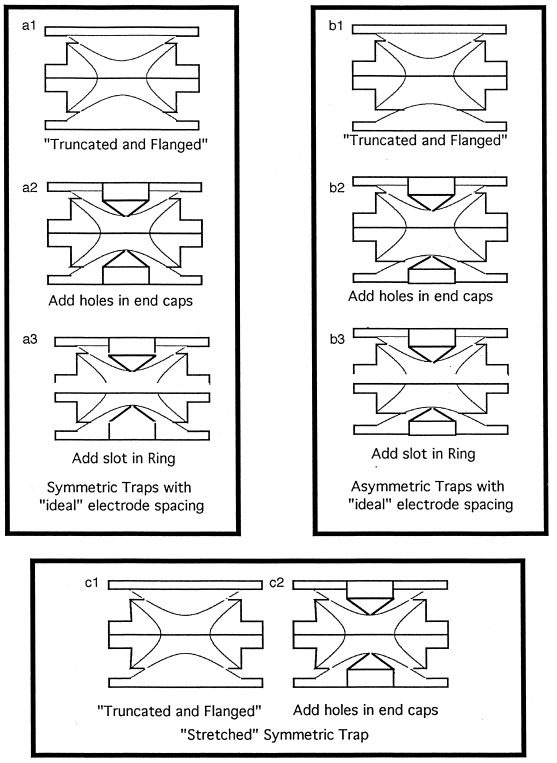

Fig. 2. Schematic illustration of hyperbolic electrode structures used for sample calculations. See the text for discussion.

3. Example: study of hyperbolic traps

As an example of the application of the techniques described previously, we have chosen to model hyperbolic traps which closely resemble actual electrode structures that we have purchased or built. Fig. 2 illustrates cross sections of traps for which we have made calculations. We started with a simple truncated hyperbola design, then added endcap holes and looked at the effects of removing a section of the central ring—the "slotted ring" [28]. (These last two geometries are very similar to ones we procured from the RM Jordan Company [29].) Next we considered the "stretched trap" where the interelectrode spacing was increased by 10.8% as was approximately standard practice until recently [11,28]. (This electrode structure closely resembles the design used by Teledyne [33].) Finally we examined the characteristics of the "asymmetric" ion trap [31], again considering the

Table 2
Calculated even order C's for nine variants of hyperbolic electrode structures

Trap type	Fig.	C_0	C_2	C_4	C_6
"Ideal" trap	...	0.5	−1	0	0
Truncated trap	2.a1	0.5007	−0.9799	$1.23\,(10)^{-4}$	$1.07\,(10)^{-3}$
+ endcap holes	2.a2	0.5010	−0.9784	$4.52\,(10)^{-3}$	$1.26\,(10)^{-2}$
+ ring slot	2.a3	0.4838	−1.0044	$-2.72\,(10)^{-2}$	$5.77\,(10)^{-2}$
Stretched trap	2.c1	0.5567	−0.8777	$-1.51\,(10)^{-2}$	$-6.40\,(10)^{-3}$
+ endcap holes	2.c2	0.5569	−0.8767	$-1.26\,(10)^{-2}$	$-1.02\,(10)^{-3}$
Asymmetric trap	2.b1	0.5007	−0.9801	$-2.26\,(10)^{-4}$	$8.02\,(10)^{-4}$
+ endcap holes	2.b2	0.5009	−0.9792	$2.13\,(10)^{-3}$	$6.72\,(10)^{-3}$
+ ring slot	2.b3	0.4818	−0.9855	$-3.07\,(10)^{-2}$	$4.61\,(10)^{-2}$

cumulative effects of truncation, endcap holes and ring slots. (The latter two designs closely resemble designs built by Alexander and Barlow [32].) Our modeling started with an "ideal" hyperbolic ion trap whose endcap spacing was $\sqrt{2}$ of the internal ring diameter. Truncation of the electrodes was as illustrated in Fig. 2 and included the mounting flanges. Holes in both endcaps were added whose diameter were 0.075 times the ring diameter. The wide slot in the center of the ring electrode was set at 0.19 times the ring diameter to match actual trap assemblies. For the case of the asymmetric trap, one endcap was set at the nominal "correct" spacing and the other was moved back and reshaped to match the harmonic equipotential in just such a way that when biassed with the opposite phase of rf and sign of dc potential a harmonic well is produced [31].

Table 2 summarizes the results for the even order terms of the eight trap electrode structures illustrated in Fig. 2, plus the C_0 and C_2 of the ideal case. The values of C_0 are, of course, of no dynamical consequence in the study of trapped ions per se, however in more general problems, e.g. externally generated ions, C_0 sets the energy scale. For our purposes, the calculation of C_0 merely provided an additional check on the correctness of our approach; typically we were able to reproduce this value to better than 1 ppm. The overall characteristics of the trap are largely determined by C_2, but for rf trapping so long as it is in the vicinity of -1, its absolute value is not critical. For work in a Penning trap, precise knowledge of C_2 is useful for absolute calibration of the system. Qualitatively, we see that the magnitudes of the nonlinear terms arising from the electrode truncation are rather modest, but of opposite sign to the C_2 term. The C_4 and C_6 terms increase when holes are placed in the endcaps. The comparison between the nominal and stretched trap geometry is particularly interesting. By increasing the spacing between the electrodes, the signs of both C_4 and C_6 change; also at the 10.8% stretch used in the calculations here, the magnitude of C_6 is reduced more than tenfold. As Franzen et al. [11] have discussed, the combined effects of the sign changes and reduction of C_6 both contribute to the improved ion trap performance that this nonintuitive step produced [28,34].

Table 3 summarizes the results for the odd order terms. The terms in parentheses are nominally zero by symmetry. Their nonzero value is a measure both of our fitting quality and choice of the $z = 0$ plane as explained previously. Because all of the values are small, we conclude that the calculations are adequate for our purposes here. In the cases of the asymmetric trap calculations, we found it necessary to adjust the origin from our original guesses slightly ($<0.0025/r_0$ or 1 grid point). The result was many orders of magnitude reduction in the values of C_1 in each case; the other C's changed by about the same absolute magnitude as C_1, which was small.

Table 4 compares some of our results with those of Franzen et al. [11]. These authors calculated the effects of truncation and compared the effect of truncation at $2r_0$ and $3r_0$. We truncated our electrodes at $2.8r_0$, to closely match the dimensions of ion traps that we actually use. With that said, the agreement between the two sets of calculations must be consid-

Table 3
Calculated odd order C's for nine variants of the hyperbolic electrode structure; numbers in parentheses are nominally zero and the asterisk denotes values that were set to zero

Trap Type	Fig.	C_1	C_3	C_5
"Ideal" trap	...	0	0	0
Truncated trap	2.a1	$(-1\,[10]^{-9})$	$(3\,[10]^{-9})$	$(3\,[10]^{-9})$
+ endcap holes	2.a2	$(-9\,[10]^{-10})$	$(3\,[10]^{-9})$	$(-2\,[10]^{-9})$
+ ring slot	2.a3	$(-2\,[10]^{-9})$	$(6\,[10]^{-9})$	$(-5\,[10]^{-9})$
Stretched trap	2.c1	$(-1\,[10]^{-9})$	$(3\,[10]^{-9})$	$(-2\,[10]^{-9})$
+ endcap holes	2.c2	$(-1\,[10]^{-9})$	$(2\,[10]^{-9})$	$(-1\,[10]^{-9})$
Asymmetric trap	2.b1	0*	$-3.06\,(10)^{-4}$	$-3.30\,(10)^{-4}$
+ endcap holes	2.b2	0*	$-1.45\,(10)^{-3}$	$-3.81\,(10)^{-3}$
+ ring slot	2.b3	0*	$-5.18\,(10)^{-3}$	$-6.55\,(10)^{-3}$

ered excellent. The small differences that do exist can all be attributed to the details of the truncation of the electrodes and differences in our approaches to evaluating the constants.

4. Discussion

The work described here was motivated by our desire to understand features associated with rf trap designs and their performance. What we have found is a general procedure for accurately extracting electrostatic potentials from relaxation calculations. The procedure can be applied to any system, but is particularly straightforward for systems which possess cylindrical symmetry. Further, the procedure here can be readily coded up thereby reducing the tedium associated with moving large files about and concern with arithmetic errors that are almost inevitable with manipulating complicated expressions. One use that we anticipate using ourselves is the investigation of precision, i.e. we would like to be able to specify the machining and assembly tolerances required to achieve a particular end. This could result in considerable savings of time and expense without compromising performance.

Gridding techniques that are considerably more sophisticated than those used in the SIMION code can improve the accuracy of the calculation [23,35]. These techniques allow one to increase the density of grid points in the vicinity of sharp changes in the boundaries and often include much more sophisticated treatments of the boundaries even when they are relatively smooth. For instance, one can examine effects of sharp edges versus chamfering of electrodes. Codes that allow for such detail are generally not easy to use, require large computational resources and are either expensive or not publicly available. Recently resources that address these issues have become more available. We hope in the future to extend our studies to take advantage of this opportunity. In particular, we will be extending our treatment to include fully three dimensional modeling where the imposition of cylindrical symmetry can be relaxed.

Table 4
Comparison of our calculations of coefficients with results published by Franzen et al. [11], see the text

Trap type	C_2	C_4	C_6
Truncated trap, here ($r = 2.8r_0$)	−0.9799	$1.23\,(10)^{-4}$	$1.07\,(10)^{-3}$
Franzen et al. [11] ($r = 3r_0$)	−1.0000	$3.66\,(10)^{-4}$	$1.90\,(10)^{-4}$
Franzen et al. [11] ($r = 2r_0$)	−0.9996	$1.36\,(10)^{-3}$	$2.01\,(10)^{-3}$
Stretched trap here	−0.8777	$-1.05\,(10)^{-2}$	$-6.40\,(10)^{-3}$
Franzen et al. [11]	−0.8940	$-1.43\,(10)^{-2}$	$-6.28\,(10)^{-3}$

Acknowledgments

The research described in this article was performed at the W.R. Wiley Environmental Molecular Sciences Laboratory, a national scientific user facility sponsored by the Department of Energy's Office of Biological and Environmental Research and located at Pacific Northwest National Laboratory. Pacific Northwest National Laboratory is operated for the U.S. Department of Energy by Battelle under contract no. DE-AC06-76RLO 1830. This work is supported in part by the U.S. Department of Energy Office of Basic Energy Sciences, Chemical Sciences Division. This work was also supported in part by the U.S. Department of Energy Fossil Energy Technology Center. A.E.T. would like to thank ERULF for summer support.

References

[1] R.C. Davidson, Physics of Nonneutral Plasma, Addison-Wesley, Redwood City, CA, 1990, Chap. 2.
[2] R. Mittleman, H. Dehmelt, S. Kim, Phys. Rev. Lett. 75 (1995) 2839.
[3] K.R. Spangenberg, Vacuum Tubes, McGraw-Hill, New York, 1948, Chaps. 5 and 13.
[4] P. Grivet, Electron Optics, Pergamon, Oxford, 1965, Chaps. 2 and 4.
[5] C. Evans, Charles Evans and Associates, Sunnyvale, CA, personal communication.
[6] R.E. March, R.J. Hughes, Quadrupole Storage Mass Spectrometry, Wiley, New York, 1989.
[7] R.K. Julian Jr., R.G. Cooks, R. March, F.A. Londry, in Practical Aspects of Ion Trap Mass Spectrometry, Vol. 1, R.E. March, J.F.J. Todd (Eds.), CRC Press, New York, 1995, Chap. 6.
[8] H.A. Bui, R.G. Cooks, J. Mass Spectrom. 33 (1998) 297.
[9] M.W. Forbes, M. Sharifi, T. Croley, Z. Lausevic, R.E. March, J. Mass Spectrom. 34 (1999) 1219.
[10] D.A. Dahl, SIMION 3D, Version 6.0, INEEL, Idaho Falls, ID, 1995.
[11] J. Franzen, R.H. Gabling, M. Schubert, Y. Wang, in Practical Aspects of Ion Trap Mass Spectrometry, Vol. 1, R.E. March, J.F.J. Todd (Eds.), CRC Press, New York, 1995, Chap. 3.
[12] X.Z. Chu, M. Holzki, R. Alheit, G. Werth, Int. J. Mass Spectrom. Ion Processes 173 (1998) 107.
[13] M.A.N. Razvi, X.Z. Chu, R. Alheit, G. Werth, R. Bluemel, Phys. Rev. A 58 (1998) R34.
[14] Maple, Waterloo Maple, Inc., Waterloo, ON, www.maplesoft.com.
[15] Mathematica, Wolfram Research, Inc, Champaign, IL, www.wolfram.com.
[16] MathCAD, Adept Scientific, Letchworth, UK, www.adeptscience.co.uk.
[17] LiveMath Computer Algebra System, Theorist Interactive, LLC, Cambridge, Massachusetts, USA. www.livemath.com.
[18] W.R. Smythe, Static and Dynamic Electricity, 3rd ed., McGraw-Hill, New York, 1968, Chaps. 3 and 5.
[19] J.D. Jackson, Classical Electrodynamics, 2nd ed., Wiley, New York, 1975, Chap. 3.
[20] P.A. Morse, H. Feshbach, Methods of Theoretical Physics, Part I, McGraw-Hill, New York, 1953, Chap. 5.
[21] M.R. Spiegel, Fourier Analysis, Schaum's Outline Series, McGraw-Hill, New York, 1974.
[22] E.C. Beatty, J. Appl. Phys. 61 (1987) 2118.
[23] G. Gabrielse, Phys. Rev. A 27 (1983) 2277; 29 (1984) 462.
[24] G. Gabrielse, L. Haarsma, S.L. Rolston, Int. J. Mass Spectrom. Ion Processes 88 (1989) 319.
[25] F.W.J. Olver, in Handbook of Mathematical Functions, M. Abramowitz, I. Stegun (Eds.), NBS Applied Math Series 55, U.S. GPO, Washington, DC, 1964, Chap. 9.
[26] G.N. Watson, A Treatise on the Theory of Bessel Functions, 2nd ed., Cambridge University Press, Cambridge, 1958, Chap. 1.
[27] C.S. Sloane, A.A. Elmoursi, Proc. IEEE Ind. Appl. Pt. 2 (1987) 1568; E.J. Davis, M.F. Buehler, T.L. Ward, Rev. Sci. Instrum. 61 (1990) 1281.
[28] J.E.P. Syka, in Practical Aspects of Ion Trap Mass Spectrometry, Vol. 1, R.E. March, J.F.J. Todd (Eds.), CRC Press, New York, 1995, Chap. 4.
[29] S.E. Barlow, M.L. Alexander, J.C. Follansbee, U.S. Patent No. 5,693,941, 1997.
[30] Potential Extraction program is available at: http://www.emsl.pnl.gov/docs/idl/software/SimionPAViewer.html.
[31] RM Jordan Company, Inc., 990 Golden Gate Terrace, Grass Valley, CA, 95945.
[32] J. Louris, personal communication.
[33] M.L. Alexander, S.E. Barlow, Proceedings of the 46th ASMS Conference on Mass Spectrometry and Allied Topics, Orlando, FL, 1998, p. 1173.
[34] J. Louris, J. Schwartz, G. Stafford, J. Syka, D. Taylor, Proceedings of the 40th ASMS Conference on Mass Spectrometry and Allied Topics, Washington, DC, 1992, p. 1003.
[35] Handbook of Grid Generation, J.F. Thompson, B.K. Soni, N.P. Weatherhill (Eds.), CRC Press, New York, 1999.